Nuclear Materials and Energy 31 (2022) 101179

Contents lists available at ScienceDirect

Nuclear Materials and Energy

journal homepage: www.elsevier.com/locate/nme

Effect of uniaxial tensile strain on binding energy of hydrogen atoms to vacancy-carbon-hydrogen complexes in α-iron

Shintaro Hirayama [a], Koichi Sato [a,*], Daiji Kato [b,c], Hirotomo Iwakiri [d], Masatake Yamaguchi [e], Yoshiyuki Watanabe [f], Takashi Nozawa [f]

[a] Graduate School of Science and Engineering, Kagoshima University, Kagoshima 890–0065 Japan
[b] National Institute for Fusion Science, Gifu 509-5202, Japan
[c] Interdisciplinary Graduate School of Engineering Sciences, Kyushu University, Kasuga, Fukuoka 816-8580, Japan
[d] Faculty of Education and Graduate School of Education, University of the Ryukyus, Okinawa 903-0213, Japan
[e] Japan Atomic Energy Agency, Ibaraki 319-1195, Japan
[f] National Institutes for Quantum and Radiological Science and Technology, Aomori 039-3212, Japan

ARTICLE INFO

Keywords:
Vacancies
Hydrogen
Iron
Tensile strain
Binding energy
Density functional theory

ABSTRACT

The hydrogen binding energy to vacancies or vacancy-carbon complexes in α-Fe under uniaxial tensile strain was calculated using the density functional theory. The solution energies of hydrogen and carbon decreased with an increase in the uniaxial tensile strain. With increasing strain, the binding energy of hydrogen atoms to vacancies also decreases; however, the binding energy of the vacancy-carbon complexes increases. The hydrogen retention was estimated under exposure to hydrogen gas. In the strained area, both the hydrogen concentration of the interstitial hydrogen atoms and the number of hydrogen atoms trapped in the vacancies increased. Therefore, hydrogen retention increased with increasing strain; however, the change in the hydrogen binding energy did not have a strong impact on the hydrogen retention. The presence of vacancies affects hydrogen retention more strongly. Although the binding energy of hydrogen atoms to vacancy-carbon complexes increased, the hydrogen retention in the Fe-C alloy was lower than that in pure Fe.

1. Introduction

In the blanket structural materials of fusion reactors, many defects and gas atoms (hydrogen isotopes and helium) are formed by atomic displacement and transmutation, respectively. The gas atoms interact with pre-existing and irradiation-induced defects [1–8]. The formation of helium bubbles leads to the degradation of the material performance [9]. The hydrogen isotopes trapped at the defects lead to an increase in the hydrogen retention. Particularly, tritium retention is a problem in the safe operation of fusion reactors. Therefore, it is important to evaluate the interactions between defects and gas atoms. In this study, we focus on the effects of hydrogen. Vacancies can capture up to six hydrogen atoms in α-Fe in first principal calculations [10–13]. The binding energy of hydrogen atoms to vacancies was almost constant for up to two trapped hydrogen atoms, and when they were more than three, it decreased with an increase in the number of trapped hydrogen atoms. The binding energy of hydrogen atoms to vacancy clusters in α-Fe has also been determined by molecular dynamics simulations [14]. The hydrogen trapping of vacancy-type defects has also been evaluated in other fusion reactor materials such as tungsten [15-18].

Reduced-activation ferritic/martensitic (RAFM) steel is a candidate for the blanket structural materials of fusion reactors. RAFM steels have many defects such as dislocations and precipitates. A high elastic strain occurred around the dislocation cores and interfaces of the precipitates. Psiachos et al. obtained the solution energy of hydrogen in α-Fe under uniaxial, hydrostatic, and shear strains and estimated the hydrogen concentration in α-Fe-containing dislocations, which led to the high solubility of hydrogen [19,20]. Ma et al. reported that strained vacancies introduced near the coherent interfaces between α-Fe and the precipitates enhanced hydrogen trapping [21]. Strain influences hydrogen retention in α-Fe. RAFM steels also include carbon atoms. Because carbon is an interstitial solute atom, it strongly interacts with vacancies. Monasterio et al. obtained the binding energies of hydrogen atoms to vacancy-carbon complexes in α-Fe using density functional theory (DFT) calculations [22]. The binding energy of a hydrogen atom to vacancies is lower than that of the vacancy-carbon complexes. The effect of carbon

* Corresponding author.
E-mail address: ksato@mech.kagoshima-u.ac.jp (K. Sato).

https://doi.org/10.1016/j.nme.2022.101179
Received 29 October 2021; Received in revised form 29 March 2022; Accepted 31 March 2022
Available online 4 April 2022

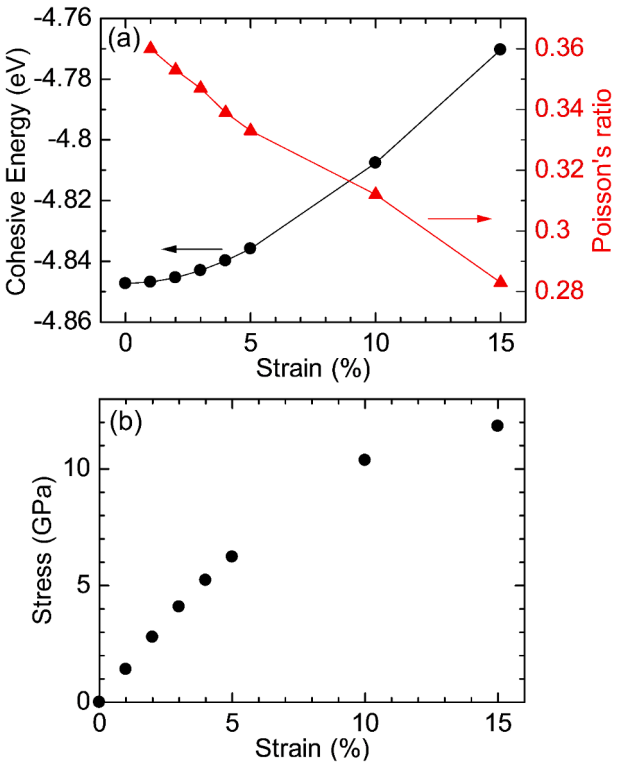

Fig. 1. (a) Calculated Poisson's ratio and cohesive energy at each strain. (b) Stress–strain curve.

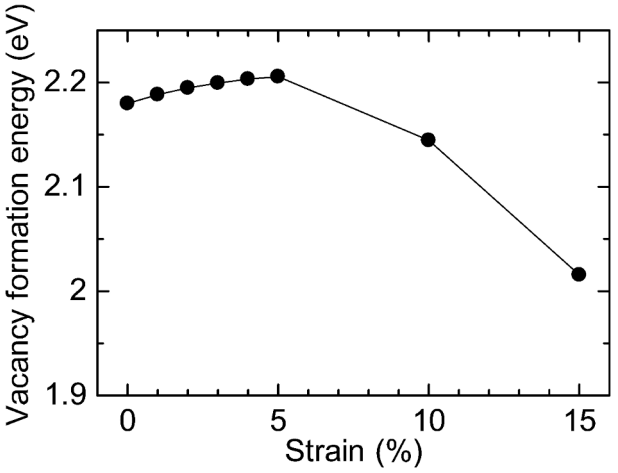

Fig. 2. Vacancy formation energy in strained α-Fe.

was also considered in estimating the number of hydrogen atoms trapped in the vacancies. Carbon may have a significant effect on the interaction between hydrogen atoms and vacancies in the strain field. Therefore, the synergistic effects of carbon and strain on this interaction should be evaluated. In this study, the hydrogen binding energy to vacancies or vacancy-carbon complexes in α-Fe under uniaxial tensile strain was calculated using DFT calculations, and the effects of uniaxial tensile strain and carbon on hydrogen retention were discussed.

2. Calculation method

A reference body-centered cubic (bcc) supercell containing 128 iron atoms was used in this study. Density functional theory (DFT) calculations were performed using plane-wave basis sets and projector-augmented wave (PAW) potentials, as implemented in the Vienna ab initio simulation package (VASP) [23–26]. For the exchange and correlation functionals, the generalized gradient approximation (GGA) in

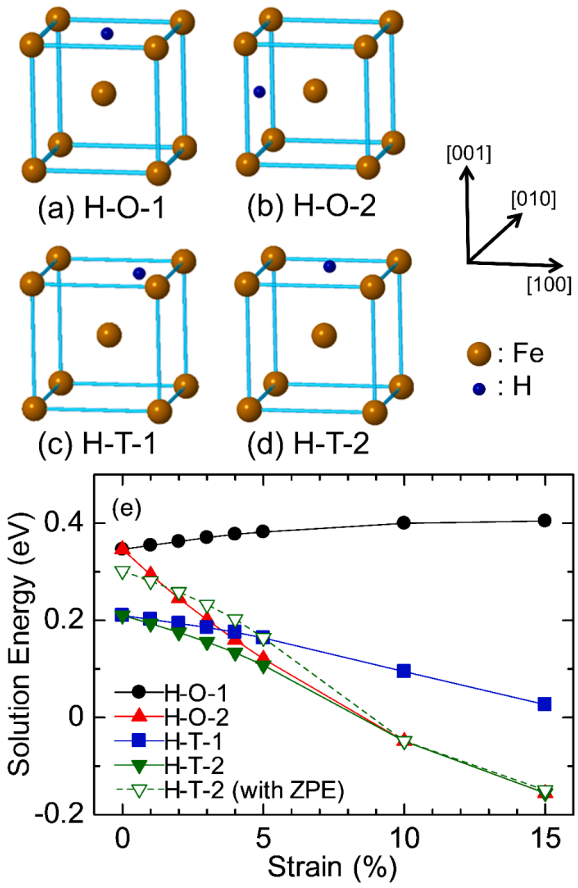

Fig. 3. Initial configuration of interstitial hydrogen atom ((a)–(d)) and solution energy of hydrogen atom at each uniaxial tensile strain (e).

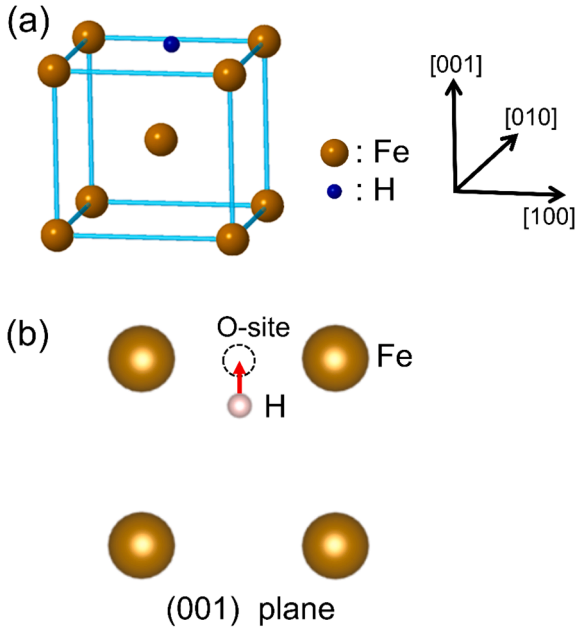

Fig. 4. (a) Configuration of interstitial hydrogen atom in H-T-2 (Fig. 3 (d)) in the strain of 5% after the lattice relaxation. (b) View from the upper side of (a).

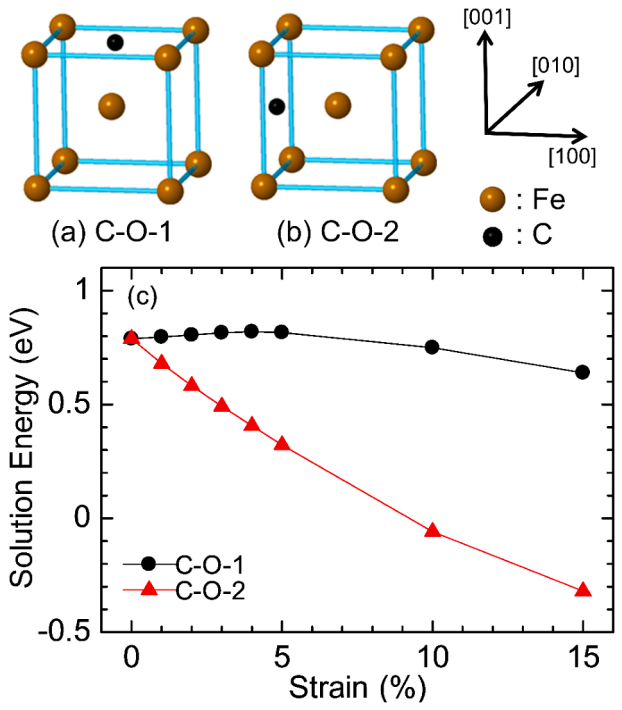

Fig. 5. Initial configuration of interstitial carbon atom ((a), (b)) and the solution energy of a carbon atom at each uniaxial tensile strain (c).

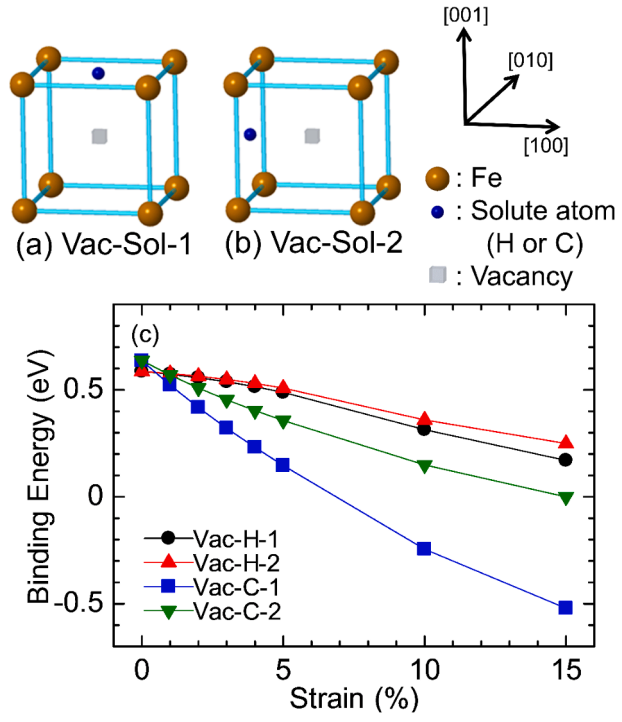

Fig. 6. Initial configuration of a vacancy-solute atom complex ((a), (b)) and the binding energy of a solute atom to a vacancy at each uniaxial tensile strain (c).

the scheme of Perdew, Burke, and Ernzerhof (PBE) was applied [27]. The cutoff energy of the plane wave basis set was set to 520 eV, and Brillouin zone integration was performed using 4 × 4 × 4 Monkhorst-Pack k-points. All atoms were fully relaxed with a total energy change of less than 10^{-6} eV, and the force on each ion was less than 0.01 eV/Å. Uniaxial tensile strains of 1, 2, 3, 4, 5, 10, and 15% were applied to the supercell in the [1 0 0] direction, and then the supercell was compressed in the [0 1 0] and [0 0 1] directions to minimize the total energy of the strained supercell. When thin foils are torn, the elastic strain in the [1 0 0] direction is greater than 10% in the fracture tips of metals immediately before the fracture [28]. Therefore, the uniaxial tensile strain in the [1 0 0] direction was applied. Fig. 1 shows the calculated Poisson's ratio and cohesive energy at each strain and stress–strain curve. The cohesive energy is the difference between the energy of an isolated iron atom in vacuum (−3.462 eV) and the total energy of the supercell divided by the total number of atoms. The cohesive energy and stress increase, and Poisson's ratio decreases with increasing strain. To calculate the total energy of the strained supercell containing defects, the cell shape and volume of the strained supercell were fixed, the defects were introduced to the strained supercell, and the atomic positions were relaxed.

The vacancy formation energy $E_f(\mathrm{Vac})$ is calculated as

$$e_f(\mathrm{Vac}) = E(\mathrm{Fe,Vac}) - E(\mathrm{Fe}) + E_c(\mathrm{Fe}), \tag{1}$$

where "Vac" denotes a vacancy, E(Fe, Vac) is the total energy of the supercell containing a vacancy, E(Fe) is the total energy of the supercell of the perfect Fe lattice, and E_c(Fe) is E(Fe) divided by the number of atoms. The solution energy of the solute atom A e_s(A) is expressed as

$$e_s(\mathrm{A}) = E(\mathrm{Fe,A}) - E(\mathrm{Fe}) - E_c(\mathrm{A}), \tag{2}$$

where E(Fe, A) is the total energy of the supercell containing solute atom A. When the solute atoms are hydrogen (A = H), E_c(H) is half of the total energy of a hydrogen molecule in vacuum. When the solute atoms are carbon (A = C), E_c(C) is the total energy of diamond divided by the number of atoms. The binding energy of the solute atom A to a defect e_B(def - A) is given as

$$e_B(\mathrm{def\ -\ A}) = E(\mathrm{Fe,def}) + E(\mathrm{Fe,A}) - E(\mathrm{Fe,\ def\ -\ A}) - E(\mathrm{Fe}), \tag{3}$$

where "def-A" denotes a defect-solute atom complex, and E(Fe, def) denotes the total energy of the supercell containing a defect. In this study, the defect was a vacancy (Vac), vacancy-hydrogen complex (Vac-H), or vacancy-carbon complex (Vac-C). The zero-point energy (ZPE) correction for hydrogen atoms was applied to some configurations. The solution energy and binding energy of hydrogen atoms, including the ZPE correction (e_s^{ZC}(H) and e_B^{ZC}(def - H)), are given as

$$e_s^{ZC}(\mathrm{H}) = e_s(\mathrm{H}) + ZPE(\mathrm{Fe,H}) - \frac{1}{2}ZPE(\mathrm{H_2}), \tag{4}$$

$$e_B^{ZC}(\mathrm{def\ -\ H}) = e_B(\mathrm{def\ -\ H}) + ZPE(\mathrm{Fe,H}) - ZPE(\mathrm{Fe,\ def\ -\ H}), \tag{5}$$

where ZPE(Fe, H) is the ZPE for an interstitial hydrogen atom in the supercell, $ZPE(\mathrm{H_2})$ is the ZPE for a hydrogen molecule in a vacuum, and ZPE(Fe, def-H) denotes the ZPE for a hydrogen atom trapped at a defect.

3. Results and discussion

Figure 2 shows the vacancy formation energy in the strained α-Fe.

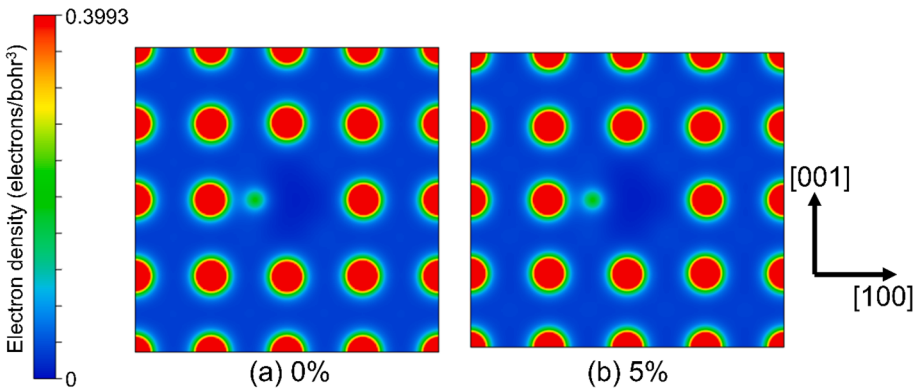

Fig. 7. Electron density distribution in Vac-H-2 (Fig. 6 (b)) without strain and with 5% strain.

The vacancy formation energy increases with an increase in the strain up to 5% and then decreases with an increase up to 15%. In many fcc metals, the vacancy formation energy obtained by DFT calculations increases with an increase in the uniaxial tensile strain up to 4% and then it decreases up to 5% [29]. The same trend was observed for fcc Cu using semi-empirical *N*-body potentials [30]. In tungsten, the vacancy formation energy increases with hydrostatic and biaxial strains up to 5% [31]. When vacancies are introduced into the dense region of the atoms, they are stable. Meanwhile, the opposite phenomenon occurred under tensile strain. Therefore, the vacancy formation energy increased with an increase in the strain up to 5%. At the strains of 10% and 15%, because interatomic bonds weaken, it is easy to introduce vacancies.

Figure 3 shows the initial configuration of an interstitial hydrogen atom ((a)–(d)) and the solution energy of a hydrogen atom at each uniaxial tensile strain (e). In H-O-1 (Fig. 3(a)), the solution energy of hydrogen increases with an increase in the tensile strain, whereas in the other configurations (Fig. 3(b)–(d)), it decreases with an increase in the tensile strain. The solution energy of hydrogen in H-T-2 is the lowest. Hydrogen atoms are more stable in the tetrahedral site (T-site) than in the octahedral site (O-site) at tensile strains of up to 5%; however, the hydrogen atom approaches the O-site after relaxation, as shown in Fig. 4. This trend agrees with a previous work [32]. The atomic distances in the [1 0 0] direction broadened, and the solute hydrogen atoms migrated to a larger space. At tensile strains of 10 and 15%, hydrogen atoms migrated from the T-site to the O-site in H-T-2. In a previous study [20], the solution energy of hydrogen decreased to approximately 0 eV under uniaxial tensile strain of approximately 4%. This is because of the different calculation conditions (the volume and shape of the supercell were fixed in this study). The solution energy of hydrogen in H-T-2, including the ZPE correction, was higher than that without the ZPE correction, and the height decreased with increasing strain. Fig. 5 shows the initial configuration of an interstitial carbon atom ((a) and (b)) and the solution energy of a carbon atom at each uniaxial tensile strain (c). Carbon atoms located at the T site migrate to the O site during lattice relaxation. Therefore, the results are omitted. The solution energy of carbon in C-O-2 was lower than that in C-O-1 and decreased with an increase in the strain. In the [1 0 0] tensile strain, the atomic distances between the carbon atom and nearest neighbor Fe atoms shortened and lengthened in C-O-1 and C-O-2, respectively.

Figure 6 shows the initial configuration of a vacancy-solute atom complex ((a) and (b)) and the binding energy of a solute atom to a vacancy at each uniaxial tensile strain (c). When the strain is applied, the distances between the Fe atoms and hydrogen atoms on the (1 0 0) plane in Vac-H-2 (Fig. 6(b)) decrease according to Poisson's ratio. Therefore, the binding energy of a hydrogen atom to a vacancy is lower in Vac-H-1 (Fig. 6(a)) than in Vac-H-2; however, the difference is not large. It decreases with an increase in the tensile strain. Almost the same trend was observed in the carbon atom; however, the value in the carbon atom was lower than that in the hydrogen atom at a strain of more than 1%. Fig. 7 shows the electron density distribution in Vac-H-2 without strain and with 5% strain. There are no noticeable differences between the 0% and 5% strains. Therefore, we obtained the site-projected partial densities of states (DOS) in the lattice not including the solute atoms, H-T-2, and Vac-H-2 without strain and with 5% strain in Fig. 8. In Fe *d*-DOS in the lattice not including solute atoms (Fig. 8(a)), the heights of the first and second prominent peaks are slightly lower, and the small peaks at approximately 6 eV (up spin) and 8 eV (down spin) above the Fermi level are slightly broader under 5% strain. In Fe *d*-DOS at H-T-2 (Fig. 8 (b)), the heights of the strong peaks did not show significant changes, but their peak positions slightly shifted to the higher energy side under 5% strain. In Fe *d*-DOS at Vac-H-2 (Fig. 8(d)), the height of the strong peaks decreased, and the positions of the small peaks at approximately 6 eV (up spin) and 8 eV (down spin) shifted to the lower energy side under 5% strain. In the H *s*-DOS at Vac-H-2 (Fig. 8(e)), the strong peaks below the Fermi level show broader profiles and a significant overlap with the Fe *d*-DOS (Fig. 8(d)) than those of H-T-2 (Fig. 8(c)). This indicates a covalent bonding character via the hybridization of the H (1 s orbital) and Fe (3d orbital) atoms. Because the peak positions shift to the lower energy side and with less overlapping with the Fe *d*-DOS under 5% strain, the covalent bonding slightly weakens. This phenomenon may lead to a decrease in the binding energy of the hydrogen atom to a vacancy associated with an increase in strain. Fig. 9 shows the initial configuration of a vacancy-two-hydrogen atom complex ((a)−(d)) and the binding energy of a hydrogen atom to a vacancy-one-hydrogen atom complex at each uniaxial tensile strain (e). In Vac-H_2-3 (Fig. 9(c)), different binding energies were obtained for two hydrogen atoms (i) and (ii). In all configurations, the binding energy of a hydrogen atom to a vacancy-H complex decreased with an increase in the strain. The binding energy of the hydrogen atom was the highest in Vac-H_2-2 (Fig. 9(b)). The highest binding energy of the hydrogen atom to a vacancy-H complex was higher than that of a vacancy (Vac-H-2) for all strains. In the distortionless condition, this result corresponds to previous works [10,12,13].

Figure 10 shows the initial configuration of the vacancy-carbon-hydrogen complex ((a)–(e)) and the binding energy of a hydrogen atom to the vacancy-carbon complex at each uniaxial tensile strain (f).

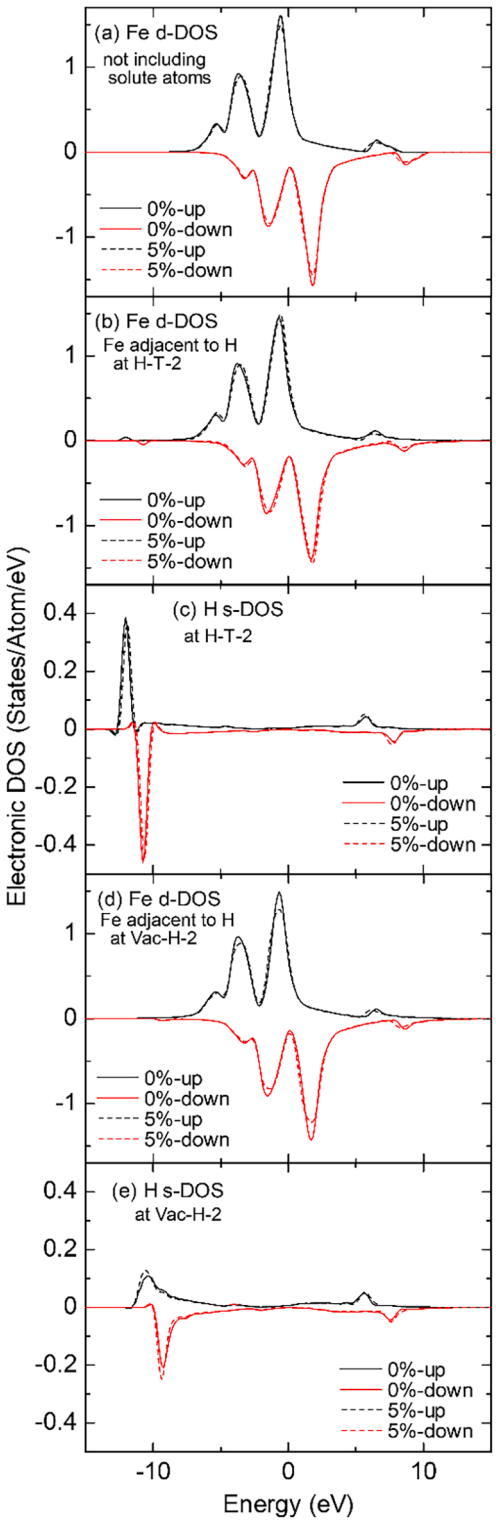

Fig. 8. Site-projected partial densities of states (DOS) in lattice not including solute atoms, H-T-2 (Fig. 3(d)), and Vac-H-2 (Fig. 6(b)) without strain and with 5% strain. In DOS, the Fermi energy is 0 eV. The solid line denotes the DOS without strain, and the dashed line represents the DOS with 5% strain. Spin up and down states have positive and negative values of DOS, respectively. Energy (gridpoint) interval is 0.13667 eV.

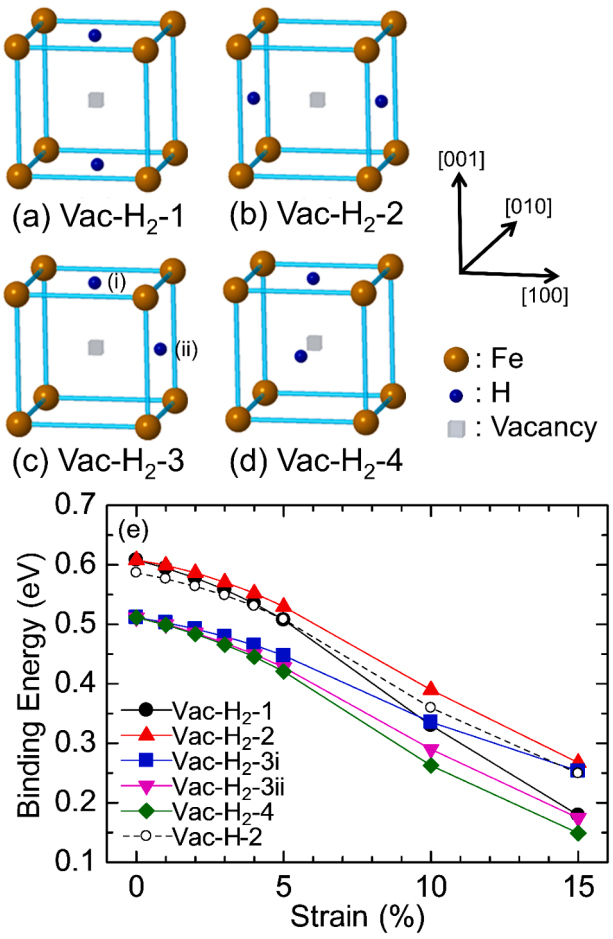

Fig. 9. Initial configuration of a vacancy-two hydrogen atoms complex ((a)–(d)) and the binding energy of a hydrogen atom to a vacancy-one hydrogen atom complex at each uniaxial tensile strain (e).

With the exception of Vac-C-H-1, the binding energy of a hydrogen atom to a vacancy-C complex decreased with an increase in the tensile strain. Only Vac-C-H-1 increased with an increase in the tensile strain. The binding energy of carbon atoms to vacancies depends on their configuration (Vac-C-1 and Vac-C-2 (Fig. 6)). To estimate the stability of Vac-C-H, the formation energy of the vacancy-carbon complex at each uniaxial tensile strain was also obtained (Fig. 11). The formation energy of Vac-C-H-1 is the lowest. Therefore, in a uniaxial strain field, the configuration of Vac-C-H-1 is the most stable. The binding energy of hydrogen in Vac-C-H-1, including the ZPE correction, was higher than that without the ZPE correction, and the difference before and after the ZPE correction decreased with an increase in the strain. The tensile strain (the increase in atomic distance) lowered the ZPE of the hydrogen atoms trapped at the vacancies. Fig. 12 shows the electron density distribution in Vac-C-H-1 (Fig. 10(a)) without strain and with 5% strain. There are no noticeable differences between the 0% and 5% strains. Therefore, we obtained the site-projected partial DOS in C-O-2 and Vac-C-H-1 without strain and with 5% strain in Fig. 13. In the Fe *d*-DOS at C-O-2 (Fig. 13- (a)) and Vac-C-H-1 (Fig. 13 (c)), the peak heights are significantly lower than those of the bulk DOS (see Fig. 8(a)) because of the hybridization between the Fe 3d and C 2p orbitals. At 5% strain, the strong peaks showed a splitting structure. The distribution of the C *p*-

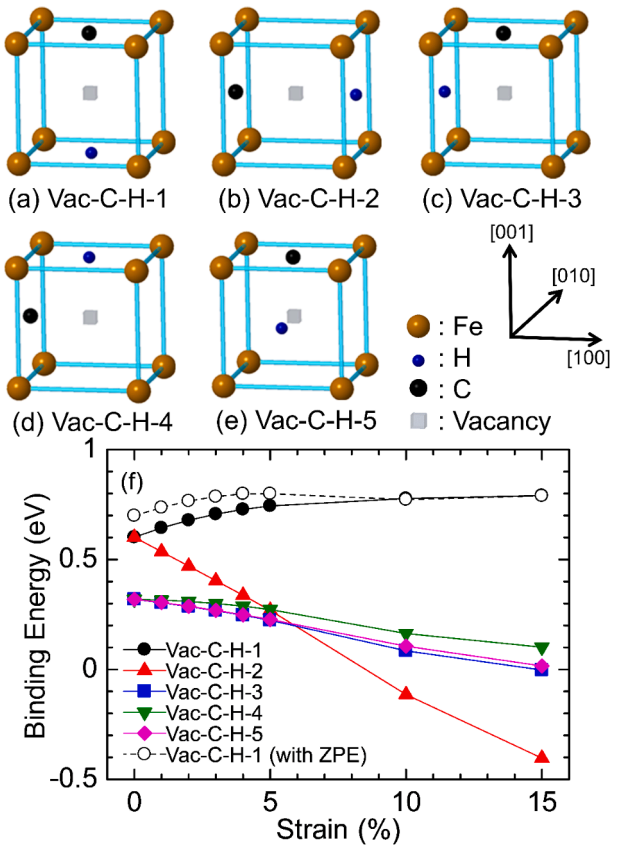

Fig. 10. Initial configuration of a vacancy-carbon-hydrogen complex ((a)–(e)) and the binding energy of a hydrogen atom to a vacancy-carbon complex at each uniaxial tensile strain (f).

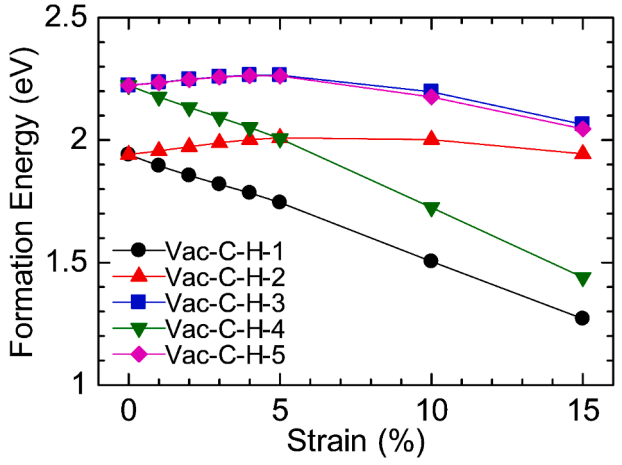

Fig. 11. Formation energy of a vacancy-carbon-hydrogen complex at each uniaxial tensile strain.

DOS at Vac-C-H-1 (Fig. 13(d)) shows broader profiles and strong overlapping with the Fe *d*-DOS. This also indicates hybridization of the C (2p orbital) and Fe (3d orbital) atoms. In the H *s*-DOS at Vac-C-H-1, the peak height of the up spin at an energy of approximately −11 eV and down spin at an energy of approximately −9 eV is slightly higher than that at Vac-H-2 (Fig. 8(e)). Therefore, the H *s*-DOS at Vac-C-H-1 may be more strongly localized than that at Vac-H-2. However, we can observe small peaks of up spin in the energy of approximately −7.5 eV and down spin in the energy of approximately −6 eV in the H *s*-DOS at Vac-C-H-1. Additionally, the shoulders appear in C *p*-DOS at Vac-C-H-1 in the energy of approximately −7.5 eV and −6 eV. These phenomena can also be ascribed to hybridization effects between H (1 s orbital) and Fe and C (2p orbital) and Fe atoms, which appear only in the vacancy-carbon-hydrogen complex. Under 5% strain, the small peaks in the H *s*-DOS are shifted to the lower energy side, and the height of the shoulders in C *p*-DOS increases and is shifted to the lower energy side. This may be correlated to the increase in the binding energy of a hydrogen atom to a vacancy-C complex associated with an increase in the strain.

We estimated the effect of strain on the number of hydrogen atoms trapped at vacancies under the following assumptions:

1. Hydrogen concentration C is calculated according to Sieverts' law [33] in the hydrogen pressure of 0.1 MPa and temperature of 300 K.
2. The number of hydrogen atoms trapped at the vacancies was obtained at local equilibrium [34]. The hydrogen occupancy θ, which indicates the number of hydrogen atoms trapped at vacancies N_H divided by the maximum value of N_H (the maximum value of N_H is equal to six in a vacancy), is given as

$$\frac{\theta}{1-\theta} = \frac{C/C_T}{1-C/C_T} exp\left[\frac{e_B(\text{def - H})}{k_B T}\right], \tag{6}$$

where C_T is the number of T sites per atom, k_B is the Boltzmann constant, and T is the absolute temperature.

3. In the Fe-carbon alloy, all vacancies capture one carbon atom.
4. When the hydrogen occupancy of a vacancy increases, the binding energy decreases [10–13]. This effect was considered in the estimation. The change in the binding energy of the hydrogen atoms to a vacancy in α-Fe is expressed by the following linear approximation:

$$e_B^{Fe}(n) = \begin{cases} 0.034n + 0.541 (0 \leqslant n \leqslant 1.93) \\ -0.127n + 0.850 (n \geqslant 1.93) \end{cases}, \tag{7}$$

where n is the number of hydrogen atoms trapped in the vacancy. For each strain, the linear function was normalized to fit $e_B^{Fe}(n=1)$ to the hydrogen binding energy obtained in this study. Here, the normalized function is given by $K{\cdot}e_B^{Fe}(n)$ (K: constant). In the Fe-carbon alloy, because a carbon atom occupies one O-site, the maximum number of hydrogen atoms trapped at a vacancy is 5. Therefore, the linear function was normalized to fit the $e_B^{Fe}(n=2)$ to the hydrogen binding energy obtained for the Fe-carbon alloy. Here, when the number of hydrogen atoms trapped in the vacancy-carbon complex is k, the normalized function is used in the Fe-carbon alloy as $K{\cdot}e_B^{Fe-C}(k) = K{\cdot}e_B^{Fe}(k+1)$ (K: constant). The approximation used in assumption 4 is summarized in Fig. 14.

5. Only vacancies exist in the materials, and they are homogeneously distributed in the strained and strain-free regions. The vacancy concentration is expressed as the C_V.
6. In these materials, only two regions (strain-free region and region strained at a strain of X%) exist. The volume ratio of the region under a uniaxial tensile strain of X% to the entire region is B. Here, B is assumed to be 0.001.

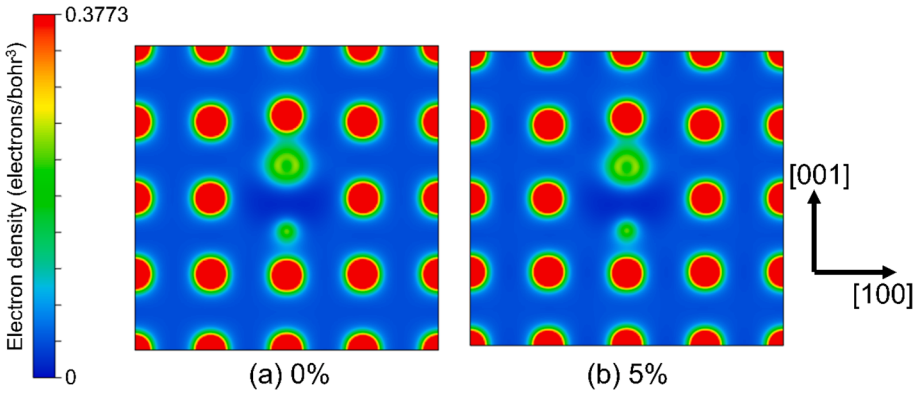

Fig. 12. Electron density distribution in Vac-C-H-1 (Fig. 10 (a)) without strain and with 5% strain.

Table 1 lists the hydrogen concentration in the homogeneously strained region (C_H), the number of hydrogen atoms trapped at vacancies in α-Fe and Fe-C alloy (N_H^{Fe} and N_H^{Fe-C}), and the total concentration of hydrogen atoms retained in the α-Fe and Fe-C alloy (C_R^{Fe} and C_R^{Fe-C}). To determine the effect of the existence of vacancies on the C_R^{Fe} andC_R^{Fe-C}, two cases ($C_V = 0$ and $C_V = 10^{-6}$) were calculated. The number of hydrogen atoms trapped at the vacancies in the Fe-carbon alloy under the uniaxial tensile strain of X% is expressed as$N_H^{Fe-C}(X)$. In this case, the total concentration of the hydrogen atoms trapped at the vacancies in α-Fe can be calculated as$\left[N_H^{Fe}(0)\cdot(1-B) + N_H^{Fe}(X)\cdot B\right]\cdot C_V$. When the uniaxial tensile strain increases, $N_H^{Fe}(X)$ increases. Consequently, the total concentration of hydrogen atoms trapped at the vacancies also increases. The total concentration of hydrogen atoms retained in α-Fe C_R^{Fe} is expressed as$C_H(0)\cdot(1-B) + C_H(X)\cdot B + \left[N_H^{Fe}(0)\cdot(1-B) + N_H^{Fe}(X)\cdot B\right]\cdot C_V$, where $C_H(X)$ is the concentration of the interstitial hydrogen atoms under the uniaxial tensile strain of X%. C_R^{Fe} and C_R^{Fe-C} are also listed in Table 1. When we compare $C_V = 0$ and $C_V = 10^{-6}$, the existence of vacancies has a significant influence on the hydrogen retention. The hydrogen retention increases with an increase in the uniaxial strain. The increase in the hydrogen retention is caused by the increase in $N_H^{Fe}(X)$ or $N_H^{Fe-C}(X)$ in the strain of 0–5%, and it is caused by the increase in $C_H(X)$ in the strain of 10 and 15%. Although the hydrogen binding energy to the vacancy-carbon complex increases with an increase in the strain, $N_H^{Fe}(X)$ is higher than$N_H^{Fe-C}(X)$. Therefore, the hydrogen retention in α-Fe is higher than that in the Fe-C alloy in the same strain. This is because carbon atoms trapped at the vacancies suppress the hydrogen trapping of vacancies. When the tensile strain reaches more than 5%, a vacancy in the Fe-C alloy can capture almost the same amount of hydrogen atoms trapped at a vacancy in the α-Fe without strain. The number of hydrogen atoms trapped at vacancies in α-Fe with 10% strain (3.58) is almost the same value in Fe-C alloy with 15% strain (3.53). Under the assumption used in this study, the effect of the uniaxial tensile strain on the hydrogen retention is not strong in materials containing vacancy-type defects; however, different kinds of strain may have a strong influence on the hydrogen retention. If materials have a broad strained area (e.g. high entropy alloys), the effect will not be neglected. Therefore, the binding energy of hydrogen atoms to vacancy-type defects is obtained under the uniaxial compressive strain, hydraulic strain, and shear strain.

4. Summary

The effect of uniaxial tensile strain on the solution energy of carbon and hydrogen and the binding energy of hydrogen to vacancy-type defects were evaluated by DFT calculations. In certain cases, the strain changed the most stable configuration. In pure Fe, the hydrogen binding energy decreases with an increase in the tensile strain. In Fe-carbon alloys, the hydrogen binding energy increased with an increase in the uniaxial tensile strain in the Vac-C-H-1. Because the carbon atoms trapped at the vacancies hindered the hydrogen trapping, the hydrogen retention in the Fe-carbon alloy was lower than that in α-Fe under the uniaxial tensile strain. In the next step, the effect of different types of strain (uniaxial compressive, hydrostatic, and shear strains) on the binding energy of hydrogen to vacancy-type defects will be evaluated to comprehensively estimate the effect of strain on hydrogen retention. Because the supercell size used in this study may be too small in the very large strain of 10 or 15%, a calculation using a larger supercell should also be attempted.

CRediT authorship contribution statement

Shintaro Hirayama: Investigation, Formal analysis, Visualization, Writing – original draft. **Koichi Sato:** Conceptualization, Investigation, Methodology, Formal analysis, Validation, Writing – original draft, Writing – review & editing. **Daiji Kato:** Investigation, Validation, Writing – review & editing. **Hirotomo Iwakiri:** Investigation, Validation, Writing – review & editing. **Masatake Yamaguchi:** Investigation, Writing – review & editing. **Yoshiyuki Watanabe:** Investigation, Validation, Resources, Writing – review & editing. **Takashi Nozawa:** Validation, Resources, Writing – review & editing.

Declaration of Competing Interest

The authors declare that they have no known competing financial interests or personal relationships that could have appeared to influence the work reported in this paper.

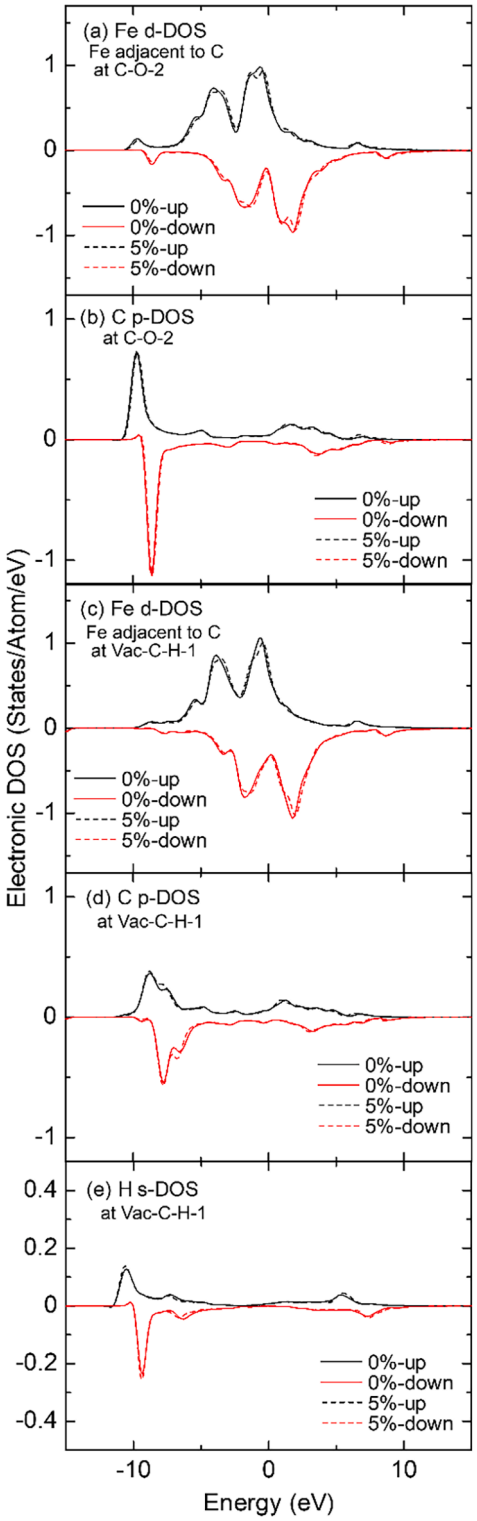

Fig. 13. Site-projected partial densities of states (DOS) in C-O-2 (Fig. 5(b)), and Vac-C-H-1 (Fig. 10(a)) without strain and with 5% strain. In DOS, the Fermi energy is 0 eV. The solid line denotes the DOS without strain, and the dashed line represents the DOS with 5% strain. Spin up and down states have positive and negative values of DOS, respectively. Energy (gridpoint) interval is 0.13667 eV.

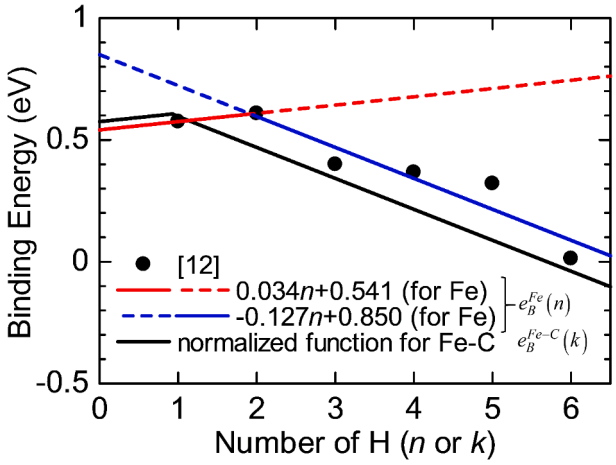

Fig. 14. Approximation used in this study. The binding energy of hydrogen atoms to a vacancy is plotted from [12].

Table 1
Hydrogen concentration in the homogeneously strained region (C_H), the number of hydrogen atoms trapped at vacancies in α-Fe and Fe-C alloy (N_H^{Fe} and N_H^{Fe-C}), and the total concentration of hydrogen atoms retained in α-Fe and Fe-C alloy (C_R^{Fe} and C_R^{Fe-C}). To determine the effect of the existence of vacancies on the C_R^{Fe} andC_R^{Fe-C}, two cases ($C_V = 0$ and $C_V = 10^{-6}$) were calculated.

Strain (%)	C_H	α-Fe			Fe-C alloy		
		N_H^{Fe}	C_R^{Fe}		N_H^{Fe-C}	C_R^{Fe-C}	
			$C_V = 0$	$C_V = 10^{-6}$		$C_V = 0$	$C_V = 10^{-6}$
0	7.31×10^{-7}	2.80	7.31×10^{-7}	4.16×10^{-6}	2.20	7.31×10^{-7}	3.27×10^{-6}
1	1.40×10^{-6}	2.86	7.32×10^{-7}	4.16×10^{-6}	2.30	7.32×10^{-7}	3.27×10^{-6}
2	2.84×10^{-6}	2.91	7.33×10^{-7}	4.16×10^{-6}	2.42	7.33×10^{-7}	3.27×10^{-6}
3	6.06×10^{-6}	2.97	7.36×10^{-7}	4.17×10^{-6}	2.52	7.36×10^{-7}	3.28×10^{-6}
4	1.42×10^{-5}	3.03	7.44×10^{-7}	4.18×10^{-6}	2.61	7.44×10^{-7}	3.29×10^{-6}
5	3.86×10^{-5}	3.10	7.69×10^{-7}	4.19×10^{-6}	2.71	7.69×10^{-6}	3.31×10^{-6}
10	1.63×10^{-2}	3.58	1.70×10^{-5}	2.04×10^{-4}	3.22	1.70×10^{-4}	1.95×10^{-4}
15	1.03	4.12	1.03×10^{-3}	1.03×10^{-2}	3.53	1.03×10^{-2}	1.03×10^{-2}

Acknowledgment

This work was performed using the JFRS-1 supercomputer system at the Computational Simulation Centre of the International Fusion Energy Research Centre (IFERC-CSC) at the Rokkasho Fusion Institute of QST (Aomori, Japan). This study was supported by the Japan Society for the Promotion of Science (JSPS) KAKENHI, Grant Numbers JP18K03584 and JP21H01068.

References

[1] P.B. Zhang, C. Zhang, R.H. Li, J. Zhao, He-induced vacancy formation in bcc Fe solid from first-principles simulation, J. Nucl. Mater. 444 (2014) 147–152, https://doi.org/10.1016/j.jnucmat.2013.09.048.
[2] P.B. Zhang, T.T. Zou, W.B. Liu, Y. Yin, J. Zhao, Stability of X-C-vacancy complexes (X=H, He) in vanadium from first principles investigations, J. Nucl. Mater. 505 (2018) 119–126, https://doi.org/10.1016/j.jnucmat.2018.04.013.
[3] C.S. Becquart, C. Domain, Ab initio calculations about intrinsic point defects and He in W, Nucl. Instrum. Meth. Phys. Res. B 255 (2007) 23–26, https://doi.org/10.1016/j.nimb.2006.11.006.

[4] C.C. Fu, F. Willaime, *Ab initio* study of helium in α-Fe: Dissolution, migration, and clustering with vacancies, Phys. Rev. B 72 (2005), 064117, https://doi.org/10.1103/PhysRevB.72.064117.
[5] P.B. Zhang, J.H. Ding, D. Sun, J. Zhao, First-principles study of noble gas atoms in bcc Fe, J. Nucl. Mater. 492 (2017) 134–141, https://doi.org/10.1016/j.jnucmat.2017.05.022.
[6] L. Yang, F. Gao, R.J. Kurtz, X.T. Zu, Atomistic simulations of helium clustering and grain boundary reconstruction in alpha-iron, Acta Mater. 82 (2015) 275–286, https://doi.org/10.1016/j.actamat.2014.09.015.
[7] Y.L. Liu, Y. Yu, Z.H. Dai, Statistical model and first-principles simulation on concentration of He_nV cluster and He bubble formation in α-Fe and W, J. Nucl. Mater. 456 (2015) 162–173, https://doi.org/10.1016/j.jnucmat.2014.09.059.
[8] D.A. Mirzaev, A.A. Mirzoev, K.Y. Okishev, A.V. Verkhovykh, Hydrogen–vacancy interaction in bcc iron: *ab initio* calculations and thermodynamics, Mol. Phys. 112 (2014) 1745–1754, https://doi.org/10.1080/00268976.2013.861087.
[9] Y. Katoh, M. Ando, A. Kohyama, Radiation and helium effects on microstructures, nano-indentation properties and deformation behavior in ferrous alloys, J. Nucl. Mater. 323 (2003) 251–262, https://doi.org/10.1016/j.jnucmat.2003.08.0.
[10] Y. Tateyama, T. Ohno, Stability and clusterization of hydrogen-vacancy complexes in a-Fe: an ab initio study, Phys. Rev. B 67 (2003), 174105, https://doi.org/10.1103/PhysRevB.67.174105.
[11] E. Hayward, C. Deo, B.P. Uberuaga, C.N. Tome, The interaction of a screw dislocation with point defects in bcc iron, Philos. Mag. Lett. 92 (2012) 2759–2778, https://doi.org/10.1080/14786435.2012.674646.
[12] K. Ohsawa, K. Eguchi, H. Watanabe, M. Yamaguchi, M. Yagi, Configuration and binding energy of multiple hydrogen atoms trapped in monovacancy in bcc transition metals, Phys. Rev. B 85 (2012), 094102, https://doi.org/10.1103/PhysRevB.85.094102.
[13] E. Hayward, C.C. Fu, Interplay between hydrogen and vacancies in α-Fe, Phys. Rev. B 87 (2013), 174103, https://doi.org/10.1103/PhysRevB.87.174103.
[14] J. Maisonneuve, T. Oda, S. Tanaka, Molecular statics study of hydrogen isotope trapping in BCC-iron vacancy clusters, Fusion Sci. Tech. 60 (2011) 1507–1510, https://doi.org/10.13182/FST11-A12718.
[15] K. Ohsawa, J. Goto, M. Yamakami, M. Yamaguchi, M. Yagi, Trapping of multiple hydrogen atoms in a tungsten monovacancy from first principles, Phys. Rev. B 82 (2010), 184117, https://doi.org/10.1103/PhysRevB.82.184117.
[16] D. Kato, H. Iwakiri, K. Morishita, Formation of vacancy clusters in tungsten crystals under htdrogen-rich condition, J. Nucl. Mater. 417 (2011) 1115–1118, https://doi.org/10.1016/j.jnucmat.2010.1.
[17] K. Ohsawa, F. Nakamori, Y. Hatano, M. Yamaguchi, Thermodynamics of hydrogen-induced superabundant vacancy in tungsten, J. Nucl. Mater. 458 (2015) 187–197, https://doi.org/10.1016/j.jnucmat.2014.12.029.
[18] N. Fernandez, Y. Ferro, D. Kato, Hydrogen diffusion and vacancies formation in tungsten: density functional theory calculations and statistical models, Acta Mater. 94 (2015) 307–318, https://doi.org/10.1016/j.actamat.2015.04.052.
[19] D. Psiachos, T. Hammerschmidt, R. Drautz, Ab initio study of the modification of elastic properties of α-iron by hydrostatic strain and by hydrogen interstitials, Acta Mater. 59 (2011) 4255–4263, https://doi.org/10.1016/j.actamat.2011.03.041.
[20] D. Psiachos, Ab initio parametrized model of strain-dependent solubility of H in α-iron, Modelling Simul. Mater. Sci. Eng. 20 (2012), 035011, https://doi.org/10.1088/0965-0393/20/3/035011.
[21] Y. Ma, Y.F. Shi, H.Y. Wang, Z.S. Mi, Z.G. Liu, L. Gao, Y. Yan, Y.J. Su, L.J. Qiao, A first-principles study on the hydrogen trap characteristics of coherent nano-precipitates in α-Fe, Int. J. Hydr. Ene. 45 (2020) 27941–27949, https://doi.org/10.1016/j.ijhydene.2020.07.123.
[22] P.R. Monasterio, T.T. Lau, S. Yip, K.J. VanVliet, Hydrogen-Vacancy Interactions in Fe-C Alloys, Phys. Rev. Lett. 103 (2009), 085501, https://doi.org/10.1103/PhysRevLett.103.085501.
[23] G. Kresse, J. Hafner, Ab initio molecular dynamics for liquid metals, Phys. Rev. B 47 (1993) 558–561, https://doi.org/10.1103/PhysRevB.47.558.
[24] G. Kresse, J. Furthmüller, Efficiency of ab-initio total energy calculations for metals and semiconductors using a plane-wave basis set, Comput. Mater. Sci. 6 (1996) 15–50, https://doi.org/10.1016/0927-0256(96)00008-0.
[25] G. Kresse, J. Furthmüller, Efficient iterative schemes for ab initio total-energy calculations using a plane-wave basis set, Phys. Rev. B 54 (1996) 11169–11186, https://doi.org/10.1103/PhysRevB.54.11169.
[26] G. Kresse, D. Joubert, From ultrasoft pseudopotentials to the projector augmented wave method, Phys. Rev. B 59 (1999) 1758–1775, https://doi.org/10.1103/PhysRevB.59.1758.
[27] J.P. Perdew, K. Burke, M. Ernzerhof, Generalized gradient approximation made simple, Phys. Rev. Lett. 77 (1996) 3865–3868, https://doi.org/10.1103/PhysRevLett.77.3865.
[28] Y. Matsukawa, K. Yasunaga, M. Komatsu, M. Kiritani, Dynamic observation of dislocation-free plastic deformation in gold thin foils, Mater. Sci. Eng. A 350 (2003) 8–16, https://doi.org/10.1016/S0921-5093(02)00689-5.
[29] Y.C. Feng, M. Liu, Y.P. Shi, H. Ma, D.Z. Li, Y. Li, L. Lu, X.Q. Chen, High-throughput modeling of atomic diffusion migration energy barrier of fcc metals, Prog. Nat. Sci.: Mater. Int. 29 (2019) 341–348, https://doi.org/10.1016/j.pnsc.2019.02.007.
[30] K. Sato, T. Yoshiie, Y. Satoh, Q. Xu, Computer simulation of formation energy and migration energy of vacancies under high strain in Cu, Mater. Trans. 45 (2004) 833–838, https://doi.org/10.2320/matertrans.45.833.
[31] Z.Z. Li, Y.H. Li, Q.Y. Ren, F.F. Ma, F.Y. Yue, H.B. Zhou, G.H. Lu, Strain dependence of energetics and kinetics of vacancy in Tungsten, Materials 13 (2020) 3375, https://doi.org/10.3390/ma13153375.
[32] H.B. Zhou, S. Jin, Y. Zhang, G.H. Lu, F. Liu, Anisotropic strain enhanced hydrogen solubility in bcc metals: the independence on the sign of strain, Phys. Rev. Lett. 109 (2012), 135502, https://doi.org/10.1103/PhysRevLett.109.135502.
[33] B.D. Morreale, M.V. Ciocco, R.M. Enick, B.I. Morsi, B.H. Howard, A.V. Cugini, K. S. Rothenberger, The permeability of hydrogen in bulk palladium at elevated temperatures and pressures, J. Membr. Sci. 212 (2003) 87–97, https://doi.org/10.1016/S0376-7388(02)00456-8.
[34] R.A. Oriani, The diffusion and trapping of hydrogen in steel, Acta Mettall. 18 (1970) 147–157, https://doi.org/10.1016/0001-6160(70)90078-7.